URSI GASS 2023, Sapporo, Japan, 19 – 26 August 2023

Neustrelitz Electron density assimilation based on 4D-Var approach: NEDAM

Liangliang Yuan* (1), Mainul Hoque (1)
(1) Institute for Solar-Terrestrial physics, German Aerospace Center (DLR), Germany; e-mail: liangliang.yuan@dlr.de

With the development of GNSS systems and the regional augmented systems, the ionospheric impact on the GNSS signals become more and more important. It is also of particular interest to retrieve the electron density distribution from GNSS observations. We have successfully developed a four-dimensional variational assimilation scheme called Neustrelitz Electron Density Assimilative Model (NEDAM) and verify NEDAM using a European ground-based GNSS network simulation. The performance of NEDAM is also investigated in a case study on 8th September 2017 using Madrigal database. The performance of NEDAM is validated against two ionosondes and COSMIC radio occultation observations during the September 2017 geomagnetic storm period. The critical frequency of F2-layer in NEDAM is much more accurate than that of the background model NEDM2020 (Neustrelitz Electron Density Model) with respect to the two ionosondes in the region of interests. During storm time, the root-mean-square error of F2-layer critical frequency with respect to the background model is improved by 0.54 and 0.42 MHz, respectively. We also compare two co-located electron density profiles retrieved from COSMIC mission with NEDAM and NEDM.

1 Introduction

It is of particular interest to retrieve the electron density distribution from Global Navigation Satellite System (GNSS) observations. There are several commonly used methods such as Computerized Ionospheric Tomography (CIT), Bayesian analysis and Kalman filter However, different methods differ in many aspects including computational cost, data storage and management cost, compatibility for different kinds of observations and flexibility in practical applications.
Several different techniques have been developed to perform posterior analyses of the ionospheric electron density. One of the traditional techniques is CIT. CIT is a direct inversion technique that develops a two-dimensional electron density specification from a series of one-dimensional ionospheric observations and various minimization criteria Similar work by other groups have led to the development of more advanced spatial analysis techniques. Howe et al. (1998) developed a Kalman filter method for the ionospheric reconstruction based upon spherical harmonics horizontally and EOFs vertically.
Bust et al. (2004) introduced IDA3D based on 4D-Var in data space. Different kinds of measurements such as GNSS TEC, ionosonde, radio occultation and in-situ measurements can be assimilated in IDA3D.

The success of data assimilation strongly relies on the accuracy of the background model and a good estimate of the background model covariances, which indicates that the assimilation results differ when using different background models. In this study, we present a real-time electron density assimilation combining different kinds of observation with the newly developed climatological electron density model Neustrelitz Electron Density Model (NEDM) for the first time. A good electron density assimilation should not only converge uniformly to the observations but also resolve the horizontal and vertical distributions of the electron densities. The accuracy of the electron density assimilation is evaluated in several aspects including all the important physical quantities such as total electron content (TEC), critical frequency of F2 layer (foF2) and corresponding peak height (hmF2).
The paper is organized as follows. Section 2 introduces four-dimensional variational data assimilation (4D-Var) and the numerical method upon which NEDAM is developed. Section 3 contains general descriptions of real GNSS data used in this study. In Section 4 we present the main initial results and discussions of NEDAM in both simulation and real data cases. In Section 5, we conclude the current status of NEDAM development as well as the future improvements.

2 Methodology

2.1 Model voxelization strategy
In NEDAM, we use a regular numerical voxelization strategy in the horizontal dimension and a nonuniform strategy in the vertical dimension. The precomputed grid has a default spacing of 2.5 degrees in latitude and 2.5 degrees in longitude. For the default spacing described above, we get total 73x145 horizontal grid points. Considering typical ionospheric profile shape, it is reasonable to construct a denser voxelization in the typical E and F region and a sparser voxelization above the F region. We assume that the vertical grid consists of around 100 elements from 60 km up to 20000 km. Vertical grid spacing is set to a high value of 10 kilometers in the ionospheric E and F region since we are interested in the hmF2 variation which may be retrieved from data assimilations. Above F2-layer a geometric series is adopted considering slowly varying vertical structure.

$$\mathrm{h}_n = h_0 + \frac{q^n - 1}{q - 1} \cdot dh \quad (1)$$

where h_n is the height of n^{th} layer, q is a scaling factor which is 1.25 here, dh is set to 20 km.

This paper's copyright is held by the author(s). It is published in these proceedings and included in any archive such as IEEE Xplore under the license granted by the "Agreement Granting URSI and IEICE Rights Related to Publication of Scholarly Work."

Considering above mentioned spatial and vertical resolutions, the total number of grid points becomes a magnitude of 10^7 in the current NEDAM configuration.

2.2 Variational problem
Following Courtier et al (1994), the cost function in 4D-Var can be written as follows,

$$J(x(t_0)) = \frac{1}{2}[(x(t_0) - x_o^b(t_0))^T B_0^{-1}(x(t_0) - x_o^b(t_0)) + \sum_k (y_k - H\mathrm{x}(t_k))^T R_k^{-1}(y_k - H\mathrm{x}(t_k))] \quad (2)$$

where $x(t_0)$ represents the analysis state variable at time t_0, $x_o^b(t_0)$ the background state variable at time t_0, B_0^{-1} the background precision matrix, y_k the observation at time t_k, H the design matrix, R_k^{-1} the observation precision matrix and $\mathrm{x}(t_k)$ the predicted state variable at time t_k. The state variable $x(t_0)$ to be analyzed could be estimated based on a minimization procedure of the cost function $J(x(t_0))$. It is commonly known to adopt the gradient or conjugate gradient method for minimizing the cost function. As long as the cost function is strictly convex and the projection from y_k to $\mathrm{x}(t_k)$ is linear, every local minimum of $J(x(t_0))$ is a global minimum.
Since the background model in this study is fully empirical, we adopt a simple forecast model for 4D-Var depending on the relative motion between the ionosphere and solid earth's rotation to the lowest order of approximation. The forecast model can be represented by a translation along the zonal direction between the earth-fixed reference frame and inertia reference frame.

$$\mathrm{x}(t_{k+1}) = \mathrm{R}(t_{k+1} - t_k)\mathrm{x}(t_k) \quad (3)$$

where R is the zonal translation matrix associated with time interval $\Delta \mathrm{t} = t_{k+1} - t_k$. The rotation forecast model is assumed to be perfect and therefore there is no weak constraint term added on the right-hand side of the cost function.

2.3 Precondition of the cost function
In most cases, it is also beneficial to use incremental form of 4D-Var in the following preconditioning procedure (Courtier et al., 1994). Substituting $x(t_0) - x_o^b(t_0)$ with $U[x(t_0) - x_o^b(t_0)]$ and $U^T U = B_0^{-1}$, since B_0^{-1} is symmetric positive definite and define $v = U[x(t_0) - x_o^b(t_0)]$ so that $[x(t_0) - x_o^b(t_0)]^T B_0^{-1}[x(t_0) - x_o^b(t_0)] = v^T v$, it allows us to re-write the cost function as follows

$$\mathrm{J}(v) = v^T \mathrm{v} + (y' - HRU^{-1}v)^T R_k^{-1}(y' - HRU^{-1}v) \quad (4)$$

where $y' = \mathrm{y} - \mathrm{HR}x_o^b(t_0)$ and the subscript k is dropped for brevity. After solving this argument v minimizing the new cost function, the original state variable ψ^a can be retrieved by

$$x^a(t_0) = U^{-1}v + x_o^b(t_0) \quad (5)$$

It is also worth noting that the preconditioning procedure reduces the computational cost of the first term of the right-hand side of the cost function (2) from $\mathrm{O}(n^2)$ to $\mathrm{O}(n^1)$.

3 Data
In this work, the data used for NEDAM are the post processed GNSS TEC provided by the MIT Haystack Observatory during September 2017 geomagnetic storms, which are available at the CEDAR Madrigal database (http://cedar.openmadrigal.org/). For the period under investigation, the database provides GNSS measurements from around 20 stations over the African region, as presented in Figure 1 at 22:00 UT on 8th September 2017 while the daily distribution can be found in the supplementary animation. The geomagnetic and interplanetary conditions were examined using the auroral electrojet index (AE), SYM-H index, three components of the Interplanetary Geomagnetic Field (IMF), solar wind plasma speed, proton temperature, and proton density measured at L1 Lagrange point by DSCOVR satellite during 6–8 September 2017 in Figure 2. These data can be found at the NASA website https://spdf.gsfc.nasa.gov/.

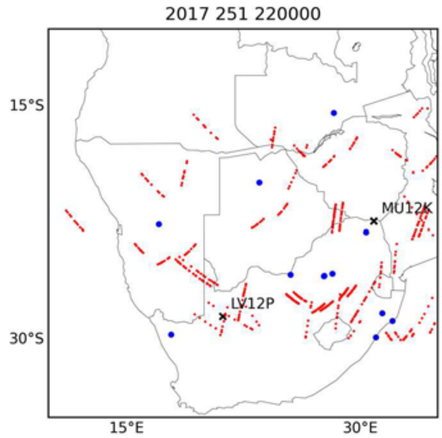

Figure 1 Geographical distributions of GNSS stations (blue dots), ionosphere pierce points of the GNSS TEC observations (red dots), and ionosonde stations MU12K and LV12P (black crosses) at 22:00 UT on 8 September 2017.

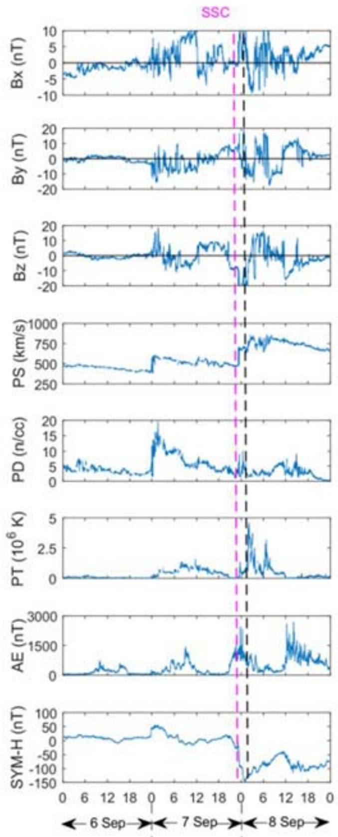

Figure 2 Space weather indices during 6–8 September 2017. The purple dashed line represents the storm sudden commencement (SSC) at 23:02 UT on September 7, 2017. The black dashed line represents the sudden increase of solar wind plasma temperature and speed.

4 Results

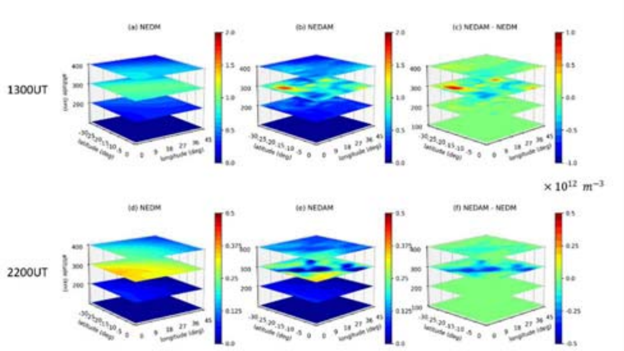

Figure 3 Horizontal slices of electron densities at 100, 200, 300, and 400 km on 8th September 2017 over African sector. (a, d) Background model (NEDM2020). (b, e) Data assimilation results using 4D-Var technique (NEDAM). c, f) Difference between NEDAM and NEDM.

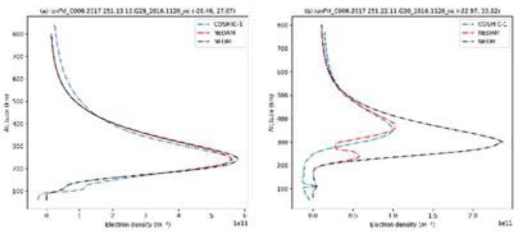

Figure 4 Comparison of electron density profiles among NEDAM, NEDM2020 and COSMIC-1 radio occultation. Panel (a) and (b) shows two radio occultation events which are co-located on 8th September 2017. The numbers in brackets of titles represent the geographical latitude and longitude of perigee points.

Figure 4 shows the comparisons of electron density profiles between NEDAM, NEDM and COSMIC-1 radio occultation. Since COSMIC-1 mission was at the end of its lifetime, only one or two satellites provided good radio occultation observations during this geomagnetic storm. Fortunately, there are two radio occultation events which are co-located. The electron density profiles from NEDAM and NEDM are interpolated to the tangent points. In figure 4a, the first radio occultation event started around 13:12 UT at 26.46S, 27.07E and the electron density profile shows a typical daytime vertical structure with one density peak at F2-layer. The general structures in these three cases are similar. But we see that the heights of F2 peak among these three profiles are almost the same while the peak densities differ. The peak density in NEDAM is slightly lower than that in NEDM, which is consistent with the COSMIC radio occultation profile though the peak density in NEDAM is slightly under-estimated. In figure 4b, the second radio occultation event started around 22:11 UT at 22.97S, 33.52E and the second electron density profile is quite different from the first one, which is probably due to the lack of daytime photonization and complicated dynamics during recovery phase of the storm. The radio occultation technique may become less accurate due to the break of local spherical symmetry during storm time. This maybe one of the reasons for the occurrence of negative electron densities below F-layer peak in Figure 4b. The single peak structure is not present in the night-time event and the overall structure is more complicated. It can be seen that peak density in NEDM is over-estimated by 2.5 times of the peak density in COSMIC profile. In addition, the peak density height is also quite different, which is around 300 km in NEDM and 350 km in COSMIC. In NEDAM, a dual-peak structure is clearly seen. The lower peak is located at around 230 km and the upper peak at around 380 km. Moreover, the peak density in NEDAM is close to that in COSMIC profile, which is around $10^{11} m^{-3}$. In both cases, the topside ionosphere electron density profile is well represented by NEDM. Drastic improvements in NEDAM of the improvements of two important parameters, i.e. NmF2 and hmF2 are shown compared with the COSMIC radio occultation.

This paper's copyright is held by the author(s). It is published in these proceedings and included in any archive such as IEEE Xplore under the license granted by the "Agreement Granting URSI and IEICE Rights Related to Publication of Scholarly Work."

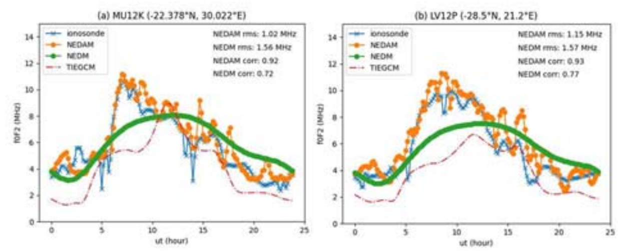

Figure 5 Comparison of peak densities (NmF2) among NEDAM, NEDM and ionosondes. Panel (a) and (d) show comparisons of NmF2 at two ionosondes, i.e. MU12K and LV12P. The TIEGCM simulation results are also plotted as red dashed lines.

In order to assess the performance of NEDAM during storm events, we compare the ionospheric electron densities with two ionosondes, i.e. MU12K (-22.37, 30.02) and LV12P (-28.5, 21.2). The ionosonde data are auto-scaled and obtained from Global Ionosphere Radio Observatory (GIRO) at https://giro.uml.edu/didbase/. Figure 5 shows the comparison of peak densities (NmF2) among NEDAM, NEDM and ionosondes. NEDM is not capable of reproducing the ionospheric response to the space weather event. The TIEGCM simulation results are also plotted as red dashed lines. In general, TIEGCM simulation results under-estimate the bottom-side electron densities generally. For MU12K case, the value of foF2 reaches its maximum at around12:00 UT in TIEGCM results. However, the maximum value of foF2 occurs around 4 hours earlier in ionosonde measurements. For LV12P case, no obvious enhancement of foF2 can be seen in TIEGCM result. In terms of improvement of foF2 in NEDAM compared to NEDM, the root mean square errors of daily foF2 decrease from 1.56 to 1.02 MHz for MU12K and from 1.57 to 1.15 MHz for LV12P. Besides the root mean square error improvement, the overall trend is also improved in NEDAM. The Pearson correlation coefficients of foF2 increase from 0.72 to 0.92 for MU12K and from 0.77 to 0.93 for LV12P despite that there are sometimes data gaps over these two ionosonde locations due to the non-uniform distribution of GNSS receivers.

5 Conclusion

We have successfully developed NEDAM, which is a four-dimensional variational assimilation (4D-Var) scheme for ionosphere electron density. We verify NEDAM using simulated data from a European ground-based GNSS network. 2. The critical frequency of F2-layer in NEDAM is much more accurate than that of NEDM when comparing with the two ionosondes in the African region. During storm time, the RMSE of critical frequency of F2 is improved by 0.54 MHz and 0.42 MHz, respectively. Furthermore, the performance of NEDAM is validated against two ionosondes and COSMIC radio occultation-derived electron density profiles during the September 2017 geomagnetic storm period. We compare the only two co-located electron density profiles from COSMIC radio occultation with NEDAM and NEDM. It is found that NEDAM is capable to reconstruct not only the peak density but also the peak density height well, which is absent in the previous research. All available real-time observations will be assimilated into NEDM in near future. And the post-processing version of NEDAM will also be introduced in near future with more kinds of observations of multiple latencies. Besides, the effect of the inclusion of measurement geometry in the observation covariances will be investigated in detail in the future. Furthermore, the successful retrieval of vertical structures strongly depends on an empirical modeling of the vertical correlation length of the ionospheric electron density, which will be investigated in details in near future.

Acknowledgements

The authors thank the Massachusetts Institute of Technology for providing access to GNSS TEC data products through the Madrigal distributed data system under support from US National Science Foundation grant AGS-1242204, COSMIC Data Analysis and Archive Center (CDAAC) for providing COSMIC-1 data. The authors also thank the Institute of Data Science of German Aerospace Center for providing High Performance Cluster.

References

[1] B. M. Howe, K. Runciman and J. A. Secan, "Tomography of the ionosphere: Four-dimensional simulations," in Radio Science, vol. 33, no. 1, pp. 109-128, Jan.-Feb. 1998, doi: 10.1029/97RS02615.

[2] Bust GS, Garner TW, Gaussiran II TL. Ionospheric Data Assimilation Three Dimensional (IDA3D): A new global, multisensor, three-dimensional electron density specification algorithm. J. Geophys. Res. 2004;109: A11312.

[3] Courtier PH, Thépaut JN, Hollingsworth A. A strategy for operational implementation of 4D-Var, using an incremental approach. Quarterly Journal of the Royal Meteorological Society. 1994 Jul;120(519):1367-87.